Journal of Solid State Chemistry 181 (2008) 1731–1737

Contents lists available at ScienceDirect

Journal of Solid State Chemistry

journal homepage: www.elsevier.com/locate/jssc

Syntheses, structures, and photoluminescence of three-dimensional lanthanide coordination polymers with 2,5-pyridinedicarboxylic acid

Yan Huang [a], Yi-Shan Song [a], Bing Yan [a,c,*], Min Shao [b]

[a] Department of Chemistry, Tongji University, Shanghai 200092, China
[b] Department of Chemistry, College of Science, Shanghai University, Shanghai 200444, China
[c] State Key Lab of Coordination Chemistry, Nanjing University, Nanjing 210093, China

ARTICLE INFO

Article history:
Received 16 December 2007
Received in revised form
21 March 2008
Accepted 31 March 2008
Available online 7 April 2008

Keywords:
Lanthanide coordination polymer
2,5-Pyridinedicarboxylate
Structure
Photoluminescent property

ABSTRACT

Four new open-framework coordination polymers of lanthanide 2,5-pyridinedicarboxylates, with the formulas Pr2(pydc)$_3$(H_2O)$_2$ (**1**), *Ln*(pydc)(Hpydc) (*Ln* = Tb (**2**), Er (**3**), Eu (**5**)), and Gd(pydc)(nic)(H_2O) (**4**) (H_2pydc = 2,5-pyridinedicarboxylic acid, Hnic = nicotinic acid), have been hydrothermally synthesized and four of them (except Eu (**5**)) have been structurally characterized. Complex **1** consists of two types of ligand-binding modes contributing to link the $PrO_7N(H_2O)$ polyhedral chains to three-dimensional (3D) open-framework architecture. Complexes **2** and **3** are isostructural and feature unique 3D cage-like supramolecular frameworks remarkably different from that of **1**, owing to the different ligand-bridging pattern. Complex **4**, however, has the distinct 3D open-framework architecture due to the presence of unexpected nicotinate ligands, which may be derived from pydc ligands via in-situ decarboxylation under the hydrothermal condition.

1. Introduction

The crystal engineering of metal-organic frameworks (MOFs) is becoming an increasingly popular field of research, owing to the potential applications and unusual topologies of these new materials [1–9]. Much work has focused on the rational design of multidimensional infinite architectures, in which the construction of transition-metal-carboxylate polymers is a successful paradigm [10–16]. Unfortunately, in contrast to the fruitful production of MOFs with *d*-block transition metal ions, the uses of lanthanide ions as nodes in the construction of MOFs are far less common and the chemistry of lanthanide coordination polymer has been less well-investigated despite their useful applications in luminescent materials [17,18], catalysis [19], etc. On the other hand, lanthanide ions, with their high and variable coordination numbers (CNs) and flexible coordination environments, are good candidates to provide unique opportunities for the discovery of unusual network topologies [20–22], so the fascinating coordination geometry and the interesting structures along with the special properties of lanthanide polymeric complexes have attracted increasing interest of chemists, and many studies have been reported in the literature recently [23–26].

An assembly of metal ions and ligands in polymeric complexes can be regarded as a programmed system in which the stereo and interactive information stored in the ligands is read by the metal ions through the algorithm defined by their coordination geometry [27,28]. Hence, the selection or design of a suitable ligand containing certain features, such as flexibility, versatile binding modes, and the ability to form hydrogen bonds [29,30], is crucial to the construction of polymeric complexes [31]. As known, lanthanide ions have high affinity for hard donor atoms, and ligands containing oxygen or hybrid oxygen–nitrogen atoms, especially pyridinecarboxylate ligands [32–38], are usually employed in the architectures for high-dimensional lanthanide polymeric complexes. 2,5-Pyridinedicarboxylic acid (H_2pydc), with divergent function groups, which could give more possibility to form bridging hydrogen bonds, is interesting and has potential for self-assembly [39]. Recent studies concerning the use of H_2pydc as a ligand toward transition metal salts [40–44] and/or lanthanide-transition metal salts [40,41] have shown that a great variety of polymeric structures can be obtained as a result of the different conformation and coordination modes of the pydc ligand. Also, H_2pydc has been proved to be a good building block for the construction of lanthanide polymers, and several open frameworks have been obtained by hydro/solvothermal reactions of H_2pydc with some lanthanide ions [35,36]. The successful isolation of these complexes prompted us to carry out the assembly of other lanthanide salts with H_2pydc under different conditions to build new coordination polymers with interesting

* Corresponding author at: Department of Chemistry, Tongji University, Shanghai 200092, China. Fax: +81 21 65982287.
E-mail addresses: byan@tongji.edu.cn, Bingyan@tongji.edu.cn (B. Yan).

0022-4596/$ - see front matter © 2008 Elsevier Inc. All rights reserved.
doi:10.1016/j.jssc.2008.03.036

structures and/or special properties for potential applications as new materials.

In addition, the hydro(solvo)thermal method has been proven to be a promising technique in the preparation of highly stable, infinite metal-ligand frameworks with much encouraging potential for applications, including nonlinear optics, catalysis and separation, magnetism, and molecular recognition [45,46]. More recently, it has been found that in-situ reactions, such as ligand hydrolysis [47,48], substitution [49], oxidative coupling [50], and decarboxylation [38], etc., can occur under hydro(solvo)thermal conditions. These reactions represent promising new routes for constructing novel coordination polymers under hydro (solvo)thermal conditions. In this contribution, we report the preparation, X-ray crystal structures and photophysical properties of four new lanthanide coordination polymers: $Pr_2(pydc)_3(H_2O)_2$ (**1**), *Ln*(pydc)(Hpydc) (*Ln* = Tb (**2**), Er (**3**)), and Gd(pydc)(nic)(H_2O) (**4**, nic = nicotinate). Surprisingly, a new ligand, nic ligand, was found to coordinate with Gd(III) in complex **4**. Since no nic ligand is present in the starting reaction mixture, it may be derived from the 2,5-pyridinedicarboxylic acid ligand via in-situ decarboxylation [38] under the hydrothermal condition. To the best of our knowledge, complex **4** presents the first example of in-situ decarboxylation in the {*Ln*/2,5-pydc} system. Besides, the selected photoluminescent properties are discussed in detail.

2. Experimental

2.1. Materials and physical measurements

$Ln(NO_3)_3 \cdot 6H_2O$ (*Ln* = Pr, Eu, Tb, Gd, and Er) were prepared by dissolving their respective oxides in concentrated nitric acid followed by drying. Other reagents were purchased commercially and used without further purification. Elemental analyses (C, H, N) were determined with an Elementar Cario EL elemental analyzer. IR spectra were recorded with a Nicolet Nexus 912 AO446 spectrophotometer (KBr pellet), 4000–400 cm^{-1} region. The powder X-ray diffraction (PXRD) was recorded on a Rigaku D/Max-2500 diffractometer at 40 kV, 100 mA for a Cu-target tube and a graphite monochromator. The luminescence (excitation and emission) spectra for the solid complex sample were obtained on a Perkin-Elmer LS-55 spectrophotometer. Luminescence lifetime measurements were carried out on an Edinburgh FLS920 phosphorimeter using a 450 W xenon lamp as the excitation source, whose lifetime data were analyzed using the Edinburgh software package. The measurements were carried out after freezing in liquid nitrogen and in argon.

2.2. Synthesis of $Pr_2(pydc)_3(H_2O)_2$ (**1**)

$Pr(NO_3)_3 \cdot 6H_2O$ (131 mg, 0.30 mmol), H_2pydc (75.2 mg, 0.45 mmol) were mixed in 5 mL deionized water. After stirring for 30 min, the mixture was placed in a 15 ml Teflon-lined reactor and heated at 160 °C in an oven for 3 days. The resulting solution was cooled slowly to room temperature; the light colorless single crystals of complex **1** suitable for X-rays four-circle diffraction analysis were obtained. Yield: 68%. Elemental analysis for **1**: $C_{21}H_{13}N_3O_{14}Pr_2$ (M_r = 813.16). Calcd: C, 40.00; H, 1.60; N, 5.17%. Found: C, 39.86; H, 1.63; N, 5.11%. IR (KBr pellet, cm^{-1}): 3430s, 1632s, 1611s, 1592s, 1482s, 1406s, 1372s, 1298m, 1250w, 1188w, 1126w, 1040m, 840w, 818w, 760m, 703m, 657w, 592m, 526m, 456w.

2.3. Synthesis of Ln(pydc)(Hpydc) (Ln = Tb (**2**), Er (**3**), Eu (**5**))

Since **2**, **3**, and **5** are isostructural, we thus present the preparation of the terbium complex. A procedure identical with that of **1** was followed to prepare **2**, **3**, and **5,** except that $Pr(NO_3)_3 \cdot 6H_2O$ was replaced by $Ln(NO_3)_3 \cdot 6H_2O$ (*Ln* = Eu, Tb, Er, 0.3 mmol). Yield: 70% (**2**), 72% (**3**) and 71% (**5**). Elemental analysis for **2**: $C_{14}H_8N_2O_8Tb$ (M_r = 491.14). Calcd: C, 34.21; H, 1.63; N, 5.70%. Found: C, 33.96; H, 1.65; N, 5.80%; for **3**: $C_{14}H_8N_2O_8Er$ (M_r = 499.63): C, 33.69; H, 1.60; N, 5.60. Found: C, 33.60; H, 1.50; N, 5.40; for **5**: $C_{14}H_8N_2O_8Eu$ (M_r = 482.33): C, 34.86; H, 1.66; N, 5.81. Found: C, 34.60; H, 1.60; N, 5.42. IR (KBr pellet, cm^{-1}) for **2**: 3439m, 1716m, 1630s, 1613s, 1582s, 1487w, 1404m, 1360m, 1282m, 1247w, 1182w, 1121w, 1034m, 834w, 813w, 756m, 700m, 652w, 587m, 521m, 452w; for **3**: 3423w, 1718m, 1630w, 1588w, 1485s, 1410s, 1366s, 1280w, 1180m, 1041m, 1035m, 835m, 762s, 692s, 650m, 537s, 440w; for **5**: 3429w, 1718m, 1630w, 1592w, 1485s, 1406s, 1372s, 1300m, 1185m, 1045m, 1036m, 904w, 835m, 791m, 767s, 686s, 650m, 529s, 428w. Comparison of the PXRD of complex **5** to the simulated XRD pattern of the reported Eu(pydc)(Hpydc) [35] shows that they are indeed the same (Fig. S1).

2.4. Synthesis of Gd(pydc)(nic)(H_2O) (**4**)

$Gd(NO_3)_3 \cdot 6H_2O$ (135 mg, 0.30 mmol), H_2pydc (75.2 mg, 0.45 mmol) were mixed in 5 mL deionized water. After stirring for 30 min, the mixture was placed in a 15 mL Teflon-lined reactor and heated at 180 °C in an oven for 3 days. The resulting solution was cooled slowly to room temperature; the light colorless single crystals of complex **4** suitable for X-rays four-circle diffraction analysis were obtained. Yield: 72%. Elemental analysis for **4**: $C_{13}H_9N_2O_7Gd$ (M_r = 462.47). Calcd: C, 33.73; H, 1.95; N, 6.05%. Found: C, 33.68; H, 1.99; N, 6.09%. IR (KBr pellet, cm^{-1}): 3469m, 3073w, 1669vs, 1608vs, 1591vs, 1578s, 1482m, 1434s, 1417s, 1400vs, 1365s, 1286w, 1178w, 1034m, 826m, 773m, 700m, 652w, 530w, 513m, 434w.

2.5. X-ray structural studies

Diffraction data of complexes **1**–**4** were collected on a Bruker SMART 1000 CCD area detector diffractometer with graphite-monochromatized Mo $K\alpha$ radiation (λ = 0.71073 Å) in the φ and ω scan modes. All the structures were solved by direct methods and refined by full-matrix least-squares methods on F^2 using the program SHELXL 97 [51]. All non-hydrogen atoms were refined anisotropically. Hydrogen atoms were placed in geometrically calculated positions. The crystallographic data and experimental details for structural analyses are summarized in Table 1. Selected bond lengths for complexes **1**–**4** are listed in Table 2.

3. Results and discussion

3.1. Syntheses

By the hydrothermal method, we have obtained complexes **1**–**3** under similar conditions at 160 °C. Compared to the Sm(III), Eu(III), and Gd(III) complexes reported before [36], complex **1** has a different structure, while complexes **2** and **3** have similar structures. To investigate the temperature dependence of lanthanide 2,5-pyridinedicarboxylate coordination polymers' structures [31], the preparative reaction was carried out at different temperatures (140, 160, and 180 °C). X-ray diffraction analyses of the products indicated that the same results were obtained at

Table 1
Crystal structure refinement data for complexes **1**–**4**

	1	2	3	4
Formula	$C_{21}H_{13}N_3O_{14}Pr_2$	$C_{14}H_8N_2O_8Tb$	$C_{14}H_8N_2O_8Er$	$C_{13}H_9N_2O_7Gd$
M_n	813.16	491.14	498.48	462.47
Temperature (K)	298(2)	273(2)	273(2)	293(2)
Crystal system	Monoclinic	Orthorhombic	Orthorhombic	Monoclinic
Space group	$P2_1/c$	*Pbcn*	*Pbcn*	$P2_1/c$
a (Å)	6.580(2)	9.9139(9)	9.8669(11)	9.249(3)
b (Å)	18.082(6)	8.6009(8)	8.5208(9)	14.181(4)
c (Å)	9.451(3)	15.7078(14)	15.6566(17)	10.529(3)
α (°)	90	90	90	90
β (°)	95.403(6)	90	90	95.738(4)
γ (°)	90	90	90	90
V (Å^3)	1119.4(7)	1339.4(2)	1316.3(2)	1374.1(7)
Z	2	4	4	4
ρ_{calcd} (g/cm^3)	2.413	2.436	2.515	2.236
μ (mm^{-1})	4.389	5.335	6.431	4.868
F(000)	780	940	948	884
GOF	0.984	1.056	1.059	0.941
R_1 [$I>2\sigma(I)$]	0.0600	0.0141	0.0142	0.0240
R_1 (all data)	0.0967	0.0158	0.0175	0.0309
wR_2 [$I>2\sigma(I)$]	0.1271	0.0341	0.0323	0.0437
wR_2 (all data)	0.1389	0.0350	0.0339	0.0452

Table 2
Selected bond lengths (Å) and bond angles (°) for complexes **1**–**4**[a]

Complex ***1***			
Pr(1)–O(1)	2.534(9)	Pr(1)–O(5)	2.454(8)
Pr(1)–O(1)#4	2.721(9)	Pr(1)–O(6)#3	2.516(8)
Pr(1) –O(2)#4	2.637(7)	Pr(1)–O(7)	2.616(8)
Pr(1) –O(3)#1	2.449(8)	Pr(1)–N(1)	2.728(8)
Pr(1) –O(4)#2	2.467(8)		
O(1)–Pr(1)–O(2)#4	90.7(3)	O(5)–Pr(1)–O(1)	82.8(3)
O(3)#1–Pr(1)–O(1)#4	78.1(2)	O(5)–Pr(1)–O(6)#3	140.4(3)
O(4)#2–Pr(1)–O(1)	71.1(2)	O(1)–Pr(1)–N(1)	61.0(2)
Complex ***2***			
Tb(1)–O(1)	2.3582(18)	Tb(1)–O(3)#4	2.3797(19)
b(1)–O(1)#3	2.3582(18)	Tb(1)–O(3)#5	2.3797(19)
Tb(1)–O(2)#1	2.3277(18)	Tb(1)–N(1)	2.558(2)
Tb(1)–O(2)#2	2.3277(18)	Tb(1)–N(1)#3	2.558(2)
O(1)#3–Tb(1)–O(1)	80.89(9)	O(3)#4–Tb(1)–O(3)#5	96.75(10)
O(2)#1–Tb(1)–O(2)#2	135.66(10)	O(1)–Tb(1)–N(1)	65.94(6)
Complex ***3***			
Er(1)–O(1)#1	2.298(2)	Er(1)–O(3)#4	2.344(2)
Er(1)–O(1)#2	2.298(2)	Er(1)–O(3)#5	2.344(2)
Er(1)–O(2)#3	2.326(2)	Er(1)–N(1)	2.520(2)
Er(1)–O(2)	2.326(2)	Er(1)–N(1)#3	2.521(2)
O(1)#1–Er(1)–O(1)#2	134.96(11)	O(3)#4–Er(1)–O(3)#5	97.67(11)
O(2)#3–Er(1)–O(2)	81.81(10)	O(2)–Er(1)–N(1)	66.68(7)
Complex ***4***			
Gd(1)–O(1)	2.369(2)	Gd(1)–O(5)	2.400(3)
Gd(1)–O(2)#1	2.386(2)	Gd(1)–O(6)	2.306(3)
Gd(1)–O(3)#3	2.443(2)	Gd(1)–O(7)#1	2.355(3)
Gd(1)–O(4)#2	2.438(2)	Gd(1)–N(1)#2	2.609(3)
O(1)–Gd(1)–O(2)#1	120.82(9)	O(4)#2–Gd(1)–N(1)#2	63.26(8)
O(6)–Gd(1)–O(7)#1	119.57(10)		

[a] Symmetry transformations for equivalent atoms: Complex **1**: #1 $-x+1,-y+2,-z+1$; #2 $-x+1,y-1/2,-z+3/2$; #3 $x-1,y,z$; #4 $x,-y+3/2,z-1/2$. Complex **2**: #1 $x+1/2,y-1/2,-z+3/2$; #2 $-x+1/2,y-1/2,z$; #3 $-x+1,y,-z+3/2$; #4 $-x+1,-y,-z+1$; #5 $x,-y,z+1/2$. Complex **3**: #1 $-x+3/2,y-1/2,z$; #2 $x-1/2,y-1/2,-z+1/2$; #3 $-x+1,y,-z+1/2$; #4 $-x+1,-y,-z+1$; #5 $x,-y,z-1/2$. Complex **4**: #1 $-x+2,-y,-z+2$; #2 $x+1,y,z$; #3 $x+1,-y+1/2,z-1/2$.

140 and 160 °C, except that the purity and yields were slightly different, indicative of the thermodynamic nature of the hydrothermal reactions. At 180 °C, however, we obtained a distinct type of Gd complex, complex **4**. It is quite surprising that single-crystal X-ray analysis of **4** illustrates the presence of nicotinate (nic) ligand in the coordination environment of Gd(III) ion. Since the nic ligand is not present in the starting reaction mixture, it may be derived from the 2,5-pyridinedicarboxylic acid ligand via in-situ decarboxylation [38] although the reactive mechanism, especially in hydrothermal or solvothermal conditions, was not clear.

3.2. Description of crystal structures

In the four complexes, there are three types of crystal structures defined as I (**1**), II (**2**, **3**), and III (**4**). All the complexes are stable in air. The IR spectra show features attributable to the carboxylate stretching vibrations of the complexes. For complexes **1**–**3**, the characteristic bands of carboxylate groups are shown in the range 1580–1632 cm^{-1} for asymmetric stretching and 1360–1490 cm^{-1} for symmetric stretching. For complex **4**, the signals in the range 1578–1669 cm^{-1} can be assigned to the asymmetric stretching vibrations for the carboxylate groups, and the signals between 1365 and 1482 cm^{-1} correspond to the symmetric stretching vibrations.

In structure I, the center metal is Pr(III) ion, and it exhibits a distorted monocapped square antiprismatic geometry by seven oxygen atoms from six pydc ligands, one nitrogen atom from one pydc ligand and one aqua ligand, as shown in Fig. 1. The Pr–O bond distances range from 2.449(8) to 2.721(9)Å with the average Pr–O separation of 2.550 Å. The Pr–N bond distance, however, is slightly longer, 2.728(8)Å.

All pydc ligands are completely deprotonated and exhibit two types of coordination modes as depicted in Chart 1a and b. It should be noteworthy that in structure I, position-1 and -4 of the pyridyl (Chart 1b) ring split into two different atoms (N and C) with 50% occupancies for each, respectively, which may be in relationship with the symmetry of the structure. The pydc ligands of the first type adopt a hexadentate chelating-bridging mode (Chart 1a) to coordinate with Pr(III) ions, forming a two-dimensional (2D) layer structure along the [100] direction (Fig. 2). In the 2D layer structure, the $PrO_7N(H_2O)$ polyhedra centers are corner-sharing through two COO^- bridges of pydc (Chart 1a) ligands, which thus create one-dimensional (1D) infinite chains (Figs. S2 and 2) with the adjacent Pr(III) separation of 4.896 Å. The pydc ligands of the other type adopt a tetradentate bridging mode (Chart 1b) to link the Pr(III) ions (Pr···Pr, 6.580 Å) from two adjacent layers to form the three-dimensional (3D) open framework (Fig. S3).

Since complexes **2** and **3** are isostructural, complex **2** is taken as an example to describe structure II in detail. Similar to the allomer of Sm, Eu, and Gd complexes [36], complex **2** crystallizes in the orthorhombic system with space group *Pbcn*, the single-crystal X-ray structural analysis shows that the structure of complex **2** is a unique 3D cage-like supramolecular framework along the [001] direction (Fig. 3). An atom numbering diagram of the fundamental unit for **2** is shown in Fig. 4. There is

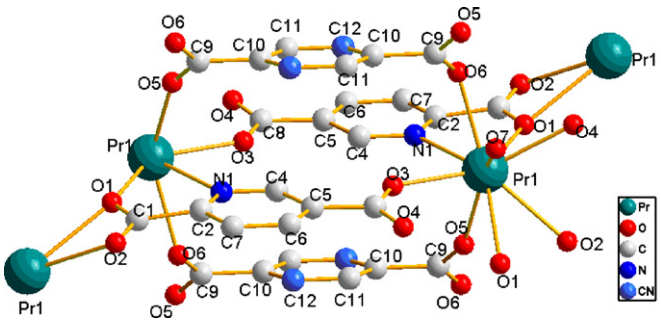

Fig. 1. Diagram showing the least asymmetry unit of **1**.

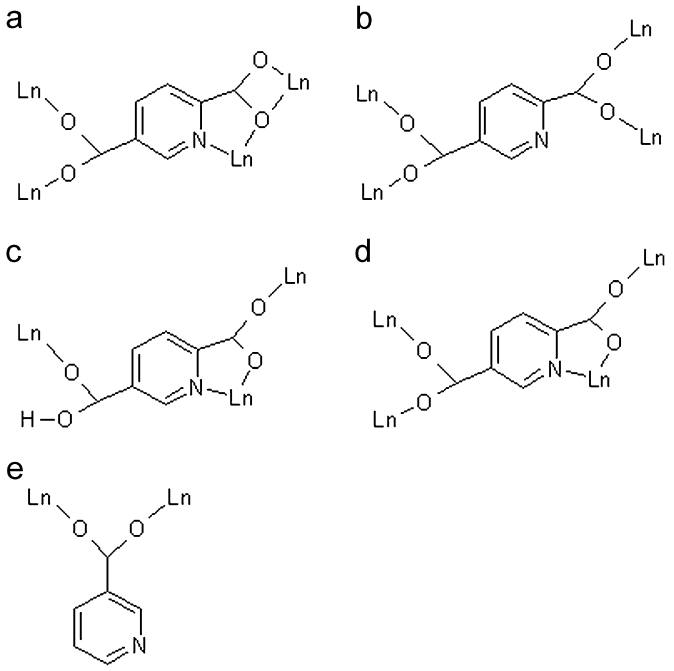

Chart 1. The coordination modes of H_2pydc and Hnic.

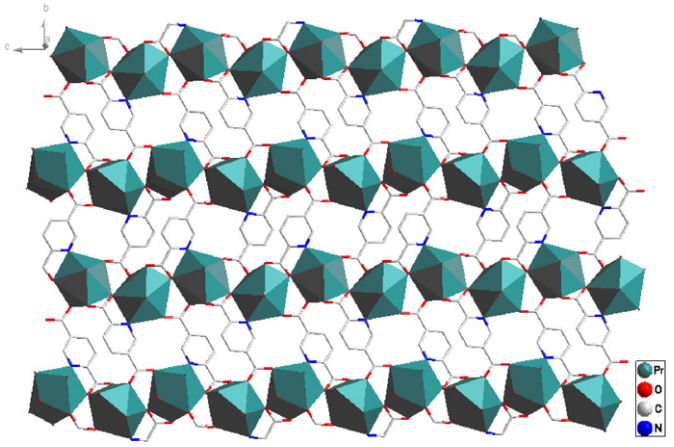

Fig. 2. The 2D layer structure of **1** formed by pydc(a) ligands linking Pr (III) ions.

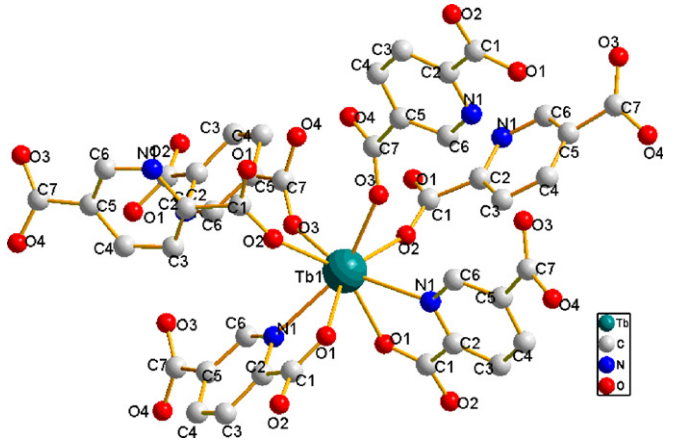

Fig. 3. The three-dimensional cage-like structure of **2** viewed down the [001] direction.

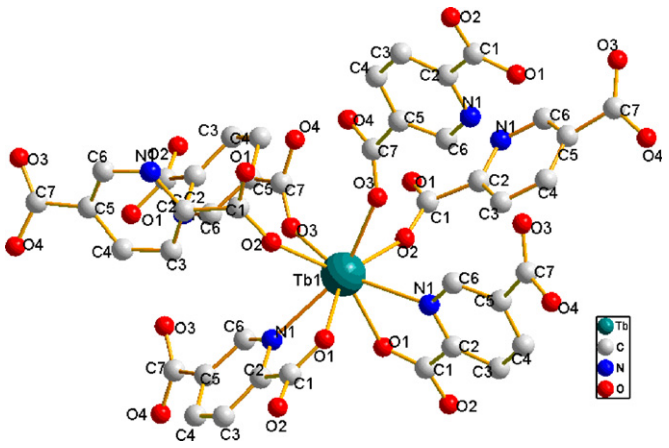

Fig. 4. Diagram showing the coordination environment of Tb (III) in **2**.

a crystallographically independent terbium ion in this structure. The local coordination geometry for the eight-coordinated Tb(III) center is close to a trigonal dodecahedron coordinated by six oxygen atoms and two nitrogen atoms from six pydc ligands. The Tb–O (carboxylate) bond distances range from 2.3277(18) to 2.3797(19)Å with the average Tb–O separation of 2.355 Å, while the Tb–N bond distance is slightly longer, 2.558(2)Å.

Unlike structure I, pydc in complex **2** adopts a tetradentate chelating-bridging coordination mode (Chart 1c). Besides linking three metal atoms, deprotonation of H_2pydc ligand is incomplete, which can be verified by the presence of a characteristic band at about 1700 cm^{-1} in the IR spectrum [36,52]. The 2-carboxylate groups of pydc ligands first link Tb centers into a helix-linked ⋯Tb–O–C–O–Tb⋯ sheet (Fig. S4), and then these sheets are cross-linked by pyridyl spacers of pydc ligands via 5-carboxylate groups into the 3D structure (Fig. S5). Moreover, it is interesting to note that two symmetry-related O4 atoms near each Tb are very close to each other (2.407 Å). Based on this, the missing H atoms would appear to be disordered over two sites between two sites [36]. And thus, an intramolecular hydrogen-bonding interaction (O(4)⋯O(4)#7 2.407(4)Å)) is formed, which plays an important role in stabilizing the uncoordinated carboxyl oxygen atoms and the whole 3D structure.

The structure of complex **4** is described in detail to introduce the structure III. A single-crystal X-ray diffraction analysis shows that complex **4** adopts a 3D framework with 1D hexagonal channels occupied by nic ligands along the [100] direction (Fig. 5). As shown in Fig. 6, there is a crystallographically independent gadolinium ion in this structure. The Gd(III) center exhibits a distorted triangle-dodecahedral configuration coordinated by six oxygen atoms from four pydc and two nic ligands (Gd–O 2.306(3)–2.443(2)Å), one nitrogen atom from one pydc ligand (Gd–N 2.609(3)Å), and one aqua ligand (Gd–O_{aqua} 2.400(3)Å).

Compared with structures I and II, the pydc ligand in complex **4** adopts a new kind of coordination mode: chelating-bridging pentadentate (Chart 1d), which is not common [36]. The nic ligand, however, adopts a bridging bidentate coordination mode with nitrogen free (Chart 1e). These bridging bidentate ends of carboxylate ligands contribute to the formation of dinuclear units, and thus, two crystallographically identical gadolinium ions are bridged by four μ_2-carboxylate ends into a dinuclear unit ($Gd_2O_{14}N_2$) with a Gd⋯Gd distance of 4.513 Å. Adjacent dinuclear units ($Gd_2O_{14}N_2$) are first linked by 2-carboxylate groups to form a 2D $Gd_2O_{14}N_2$ dinuclear-carboxylate layer (Fig. 7), and then these layers are cross-linked by pyridyl spacers of pydc ligands via 5-carboxylate groups into the 3D structure (Fig. S6). Interestingly, when viewed along the *a*-axis, the 3D network contains 1D

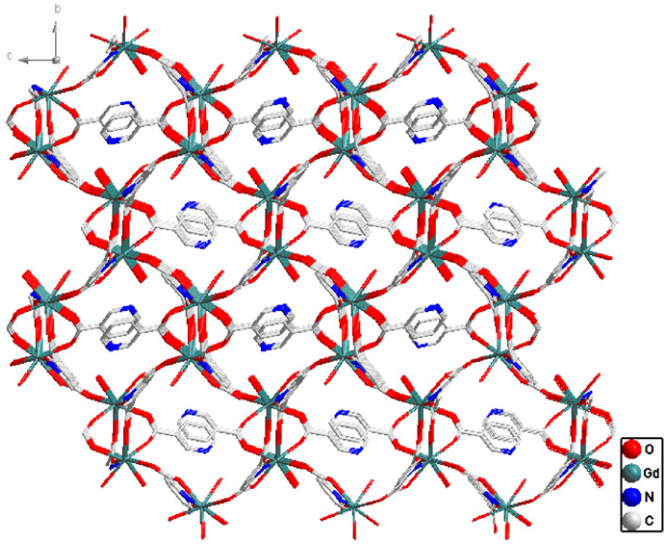

Fig. 5. View of the three-dimensional structure of **4** along the *a*-axis, showing the one-dimensional hexagonal channels occupied by one-end-coordinated nic ligands.

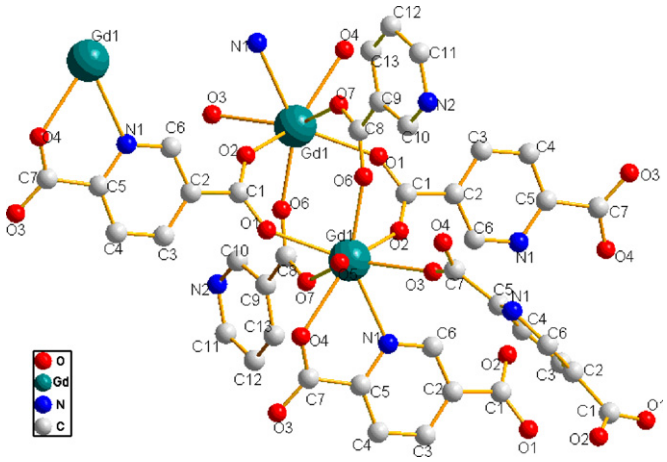

Fig. 6. Diagram showing the least asymmetry unit of **4**.

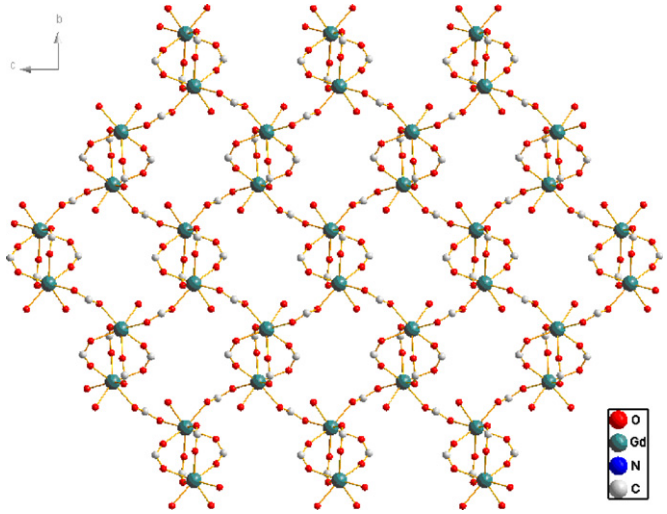

Fig. 7. The 2D $Gd_2O_{14}N_2$ dinuclear unit carboxylate layer in **4**.

hexagonal channels that are occupied by one-end-coordinated nic ligands (see Figs. 5 and S7).

3.3. Comparison of the structures

In this work, the use of various lanthanide nitrates has given rise to different types of architectures of the resultant products. In structure I, the CN of the Pr(III) ion is nine, and there are two types of Ligand-binding modes in the structure. Six pydc ligands and one aqua ligand provide eight oxygen atoms and one nitrogen atom to coordinate with the metal ion and extend the metal-organic subnetworks to the 3D open-framework structure. Complexes **2**, **3** and the allomer of Sm, Eu, and Gd complexes [36] compose structure II. In structure II, however, the CN of *Ln*(III) ions is eight, and there is only one different ligand conformation. There are six pydc ligands coordinating to the metal ions with six oxygen atoms and two nitrogen atoms, which result in 3D cage-like architectures. This phenomenon is presumably a manifestation of the well-known effect of lanthanide contraction and has some dramatic effects on crystal architectures considering the similar lanthanide-organic hybrid frameworks reported in the literature [53]. For complex **4**, however, the presence of nic ligands, which may be derived from pydc ligands via in-situ decarboxylation under the hydrothermal condition, led to a distinct type of structure, structure III. In structure III, the CN of Gd(III) ion is eight, and the pydc ligands adopt only a distinct chelating-bridging pentadentate coordination mode. Four pydc ligands, two nic ligands and one aqua ligand provide seven oxygen atoms, and one nitrogen atom coordinating to the metal ions, which result in the 3D open-framework architecture featuring hexagonal channels. It is noteworthy that the nic ligands act as terminal ligands contributing to the formation of dinuclear Gd units, and then 2-carboxylate groups linked them into 2D subnetworks, which are similar with that of structure II. But, owing to the different coordination environment of metal centers and the different coordination mode of 5-carboxylate groups, structure III finally presents a different architecture from that of structure II. Another noteworthy aspect is that complex **4** has the similar architecture with that of [*Ln*(pydc)(bc)(H_2O)] [36] (*Ln* = Sm, Gd; H_2pydc = 2,5-pyridinedicarboxylic acid; Hbc = benzenecarboxylic acid). Close inspection of these two similar architectures reveals that the nic ligand adopts the same coordination mode with that of the bc ligand and the coordination mode of pydc ligands are also same in the two types of structure, which then generates the similar contribution to the construction of the resultant architecture. This phenomenon is not common in MOFs. In addition, no solvent molecule is directly connected to the frameworks of **2** and **3**, which would be a useful feature to produce functional luminescent materials considering the quenching effect of –OH oscillators on luminescence [36].

3.4. Photoluminescent properties

Complex **2** exhibits bright green photoluminescence of Tb(III) upon the radiation of UV light in the polycrystalline state at room temperature. As shown in Fig. S8 (inner plot), a broad excitation band ranging in 220–340 nm appears with maximum excitation peak of 306 nm, corresponding to the absorption of 2,5-pydc ligand, which is favorable for the energy absorption and luminescence of Tb^{3+}. Besides, some apparent sharp excitation bands can be observed in the range of 340–390 nm with peaks at 349, 366, and 374 nm, respectively, which can be attributed to the *f*–*f* transition of Tb^{3+}. The corresponding emission spectrum (Fig. S8 (outer plot)) of complex **2** under excitation at 366 nm shows four emission bands: 493, 542 (552), 583 (589) and

621 nm, which is originated from the characteristic emission $^5D_4 \rightarrow {}^7F_J$ ($J = 6, 5, 4, 3$) transition of the Tb(III) ion. Among the characteristic emission transitions, the $^5D_4 \rightarrow {}^7F_5$ transition exhibits the strongest green emission, and the $^5D_4 \rightarrow {}^7F_6$ transition shows the second strongest blue emission. Fig. S9 presents the excitation (inner plot) and emission spectra (outer plot) of complex 5, which shows bright red emission of Eu(III) upon the radiation of UV light in the polycrystalline state at the room temperature. The wide excitation band at the range of 220–350 nm originates from the main absorption of the 2,5-pydc ligand, whose maximum excitation peak is located at 297 nm. The strong absorption of the ligand will benefit the energy absorption and transfer to Eu^{3+}. There exist apparent narrow excitation bands in the long-wavelength ultraviolet–visible region (350–420 nm) with peaks at 359, 381, 392, 412, and 416 nm, which can be ascribed to the *f–f* transition of Eu^{3+}. Under excitation at 392 nm, five main emission bands with some splits occur: 493, 542 (552), 583 (589), and 621 nm, which originate from the characteristic emission $^5D_0 \rightarrow {}^7F_J$ ($J = 0, 1, 2, 3, 4$) transition of the Eu(III) ion. Among the characteristic emission transitions, the $^5D_0 \rightarrow {}^7F_2$ transition exhibits the strongest red emission, and $^5D_0 \rightarrow {}^7F_1$ transition shows the second strongest orange emission. With respect to 2,5-H_2pydc, the emission broadband mainly ranges from 350 to 450 nm with one peak at 392 nm [34]. The absence of the ligand-based emission in the emission spectrum of **2** suggests that the energy transfer from the ligand to the lanthanide center is effective [35]. The $^5D_0 \rightarrow {}^7F_0$ transition of Eu^{3+} presents only one peak at 577 nm with no split, suggesting only one coordination environment for Eu^{3+} in complex **5**, which is in agreement with the molecular structure [36]. The luminescent intensities for both Eu and Tb complexes are strong from the corrected integrated area, suggesting there exist suitable energy match and effective energy transfer between 2,5-H_2pydc and Eu^{3+} (Tb^{3+}). Certainly no coordinated water molecules in the molecular framework is also the important reason to achieve the strong emission for no hydroxyl group from water molecules produces the non-radiative energy loss.

In addition, the experimental decay curves of complexes **2** and **5** fit well with single-exponential decay ($Ln(S(t)/S_0) = -k_1 t = -t/\tau$) (Fig. S10), indicating that Eu^{3+} or Tb^{3+} ions have one coordination environment. The lifetimes of 1.18 ms for **2** and 1.45 ms for **5** have been obtained, which is long (especially for **5**) comparable with other corresponding lanthanide complexes. This fact may be ascribed to the fact that there are no coordinated water molecules and the non-radiative loss can be avoided. Furthermore, we determined the corresponding quantum efficiency for Eu^{3+}'s $^5D_0$ emission of compound **5**. We selectively determined the emission quantum efficiencies of the $^5D_0$ europium ion excited state for the Eu^{3+} complex on the basis of the emission spectra and lifetimes of the $^5D_0$ emitting level using the four main equations according to Refs. [54–56].

$$A_{0J} = A_{01}(I_{0J}/I_{01})(\upsilon_{01}/\upsilon_{0J}) \quad (1)$$

$$A_{\mathrm{rad}} = \sum A_{0J} = A_{00} + A_{01} + A_{02} + A_{03} + A_{04} \quad (2)$$

$$\tau = A_{\mathrm{rad}}^{-1} + A_{\mathrm{nrad}}^{-1} \quad (3)$$

$$\eta = A_{\mathrm{rad}}/(A_{\mathrm{rad}} + A_{\mathrm{nrad}}) \quad (4)$$

Here A_{0J} is the experimental coefficients of spontaneous emissions, A_{01} is Einstein's coefficient of spontaneous emission between the $^5D_0$ and $^7F_1$ energy levels, which can be determined to be 50 s^{-1} approximately [54–56] and as a reference to calculate the value of other A_{0J}. *I* is the emission intensity and can be taken as the integrated intensity of the $^5D_0 \rightarrow {}^7F_J$ emission bands [54–56]. υ_{0J} refers to the energy barrier and can be determined from the emission bands of Eu^{3+}'s $^5D_0 \rightarrow {}^7F_J$ emission transitions. A_{rad} and A_{nrad} are the radiative transition rate and nonradiative transition rate, respectively, A_{rad} can be determined from the summation of A_{0J} (Eq. (2)). And the luminescence quantum efficiency (22.4%) for **5** can be calculated from the luminescent lifetimes, radiative and nonradiative transition rates. The quantum efficiency (22.4%) does not seem satisfactory in spite of the long lifetime (1.45 ms) of europium complex without coordinated water molecules, which may be due to the low red/orange ratio for the emission spectrum of complex **5**. On the basis of Eqs. (1)–(4), it can be predicted that the luminescent quantum efficiency mainly depends on two factors, one is lifetime, the other is the red/orange ratio. The emission spectrum of complex **5** indicates that the red/orange ratio is only 1.92, which is low compared to the general europium systems, resulting in the low quantum efficiency value.

4. Conclusions

In summary, we have successfully synthesized four new 3D lanthanide 2,5-pydc coordination polymers with three types of structures. In the three types of structures, H_2pydc ligands show four kinds of coordination modes. Tb and Er complexes have unique 3D cage-like supramolecular frameworks remarkably different from that of the Pr complex; for the Gd complex, however, the presence of nic ligands, which may be derived from pydc ligands via in-situ decarboxylation under the hydrothermal condition, led to the formation of a distinct type of structure featuring hexagonal channels. Besides, complexes **2** and **5** show strong characteristic luminescence of Tb and Eu ions and long lifetimes because no coordinated water molecule exists in the molecular framework and the non-radiative energy loss can be avoided. However, the low red/orange ratio for complex **5** decreases the quantum efficiency despite the long lifetime.

5. Supplementary material

Crystallographic data for the four complexes in this paper have been deposited at the Cambridge Crystallographic data center, CCDC nos. 295237, 658559, 658561 and 658560 are for complexes **1**–**4**, respectively. These data can be obtained free of charge at http://www.ccdc.cam.ac.uk/conts/retrieving-.html (or from the Cambridge Crystallographic Data Center, 12 Union Road, Cambridge CB2 1EZ, UK; fax: (+44) 1223-336-033; e-mail: deposit@ccdc.cam.ac.uk).

Acknowledgments

The authors gratefully acknowledged the financial support from the National Natural Science Foundation of China (20671072).

Appendix A. Supplementary material

Supplementary data associated with this article can be found in the online version at doi:10.1016/j.jssc.2008.03.036.

References

[1] J.S. Seo, D. Whang, H. Lee, S.I. Jun, J. Oh, Y.J. Jeon, K. Kim, Nature 404 (2000) 982–986.

[2] B. Chen, M. Eddaoudi, S.T. Hyde, M. O'Keeffe, O.M. Yaghi, Science 291 (2001) 1021–1023.
[3] O. Kahn, C. Martinez, Science 279 (1998) 44–48.
[4] E.J. Cussen, J.B. Claridge, M.J. Rosseinsky, C.J. Kepert, J. Am. Chem. Soc. 124 (2002) 9574–9581.
[5] C.Y. Su, A.M. Goforth, M.D. Smith, P.J. Pellechia, H.C. zur Loye, J. Am. Chem. Soc. 126 (2004) 3576–3586.
[6] C. Janiak, Dalton Trans. (2003) 2781–2804.
[7] F. Millange, C. Serre, G. Ferey, Chem. Commun. (2002) 822–823.
[8] Q. Wei, M. Nieuwenhuyzen, F. Meunier, C. Hardacre, S.L. James, Dalton Trans. (2004) 1807–1811.
[9] W. Zhao, J. Fan, T.A. Okamura, W.Y. Sun, N. Ueyama, New J. Chem. 28 (2004) 1142–1150.
[10] C.N.R. Rao, S. Natarajan, R. Vaidhyanathan, Angew. Chem. Int. Ed. 43 (2004) 1466–1496.
[11] L. Pan, H. Liu, X. Lei, X. Huang, D.H. Olson, N.J. Turro, J. Li, Angew. Chem. Int. Ed. 42 (2003) 542–546.
[12] A. Galet, M.C. Munoz, A.J. Real, J. Am. Chem. Soc. 125 (2003) 14224–14225.
[13] J.P. Zhang, Y.Y. Lin, X.C. Huang, X.M. Chen, J. Am. Chem. Soc. 127 (2005) 5495–5506.
[14] T.J. Prior, D. Bradshaw, S.J. Teat, M.J. Rosseinsky, Chem. Commun. (2003) 500–501.
[15] X.L. Wang, C. Qin, E.B. Wang, Y.G. Li, C.W. Hu, L. Xu, Chem. Commun. (2004) 378–379.
[16] J.K. Cheng, Y.B. Chen, L. Wu, J. Zhang, Y.H. Wen, Z.J. Li, Y.G. Yao, Inorg. Chem. 44 (2005) 3386–3388.
[17] S. Capecchi, O. Renault, D.G. Moon, M. Halim, M. Etchella, P.J. Dobson, O.V. Salata, V. Christou, Adv. Mater. 12 (2000) 1591–1594.
[18] D. Parkar, Coord. Chem. Rev. 205 (2000) 109–130.
[19] T.E. Gier, X. Bu, P. Feng, G.D. Stucky, Nature 395 (1998) 154–157.
[20] W.S. Liu, T.Q. Jiao, Y.Z. Li, Q.Z. Liu, M.Y. Tan, H. Wang, L.F. Wang, J. Am. Chem. Soc. 126 (2004) 2280–2281.
[21] G. Mancino, A.J. Ferguson, A. Beeby, N.J. Long, T.S. Jones, J. Am. Chem. Soc. 127 (2005) 524–525.
[22] F. Luo, Y.X. Che, J.M. Zheng, Cryst. Growth Des. 6 (2006) 2432–2434.
[23] D.L. Long, A.J. Blake, N.R. Champness, M. Schoder, Chem. Commun. (2000) 1369–1370.
[24] Y.C. Liang, R. Cao, W.P. Su, M.C. Hong, W.J. Zhang, Angew. Chem. Int. Ed. 39 (2000) 3304–3307.
[25] B.Q. Ma, D.S. Zhang, S. Gao, T.Z. Jin, C.H. Yun, G.X. Xu, Angew. Chem. Int. Ed. 39 (2000) 3644–3646.
[26] Y.S. Song, B. Yan, Inorg. Chim. Acta 358 (2005) 191–195.
[27] J.M. Lehn, Supramolecular Chemistry Concepts and Perspectives, VCH, Weinheim, 1995.
[28] R. Cao, D.F. Sun, Y.C. Liang, M.C. Hong, K. Tatsumi, Q. Shi, Inorg. Chem. 41 (2002) 2087–2094.
[29] C.S. Hong, S.K. Son, Y.S. Lee, M.J. Jun, Y. Do, Inorg. Chem. 38 (1999) 5602–5610.
[30] B. Moulton, M.J. Zaworotko, Chem. Rev. 101 (2001) 1629–1658.
[31] A.K. Cheetham, C.N.R. Rao, R.K. Feller, Chem. Commun. (2006) 4780.
[32] B. Zhao, L. Yi, Y. Dai, X.Y. Chen, P. Cheng, D.Z. Liao, S.P. Yan, Z.H. Jiang, Inorg. Chem. 44 (2005) 911–920.
[33] S.K. Ghosh, P.K. Bharadwaj, Inorg. Chem. 44 (2005) 3156–3161.
[34] Y.S. Song, B. Yan, Z.X. Chen, J. Mol. Struct. 750 (2005) 101–108.
[35] Y.G. Huang, B.L. Wu, D.Q. Yuan, Y.Q. Xu, F.L. Jiang, M.C. Hong, Inorg. Chem. 46 (2007) 1171–1176.
[36] C. Qin, X.L. Wang, E.B. Wang, Z.M. Su, Inorg. Chem. 44 (2005) 7122–7129.
[37] D. Min, S.W. Lee, Inorg. Chem. Commun. 5 (2002) 978–983.
[38] Z.B. Han, X.N. Cheng, X.F. Li, X.M. Chen, Z. Anorg. Allg. Chem. 631 (2005) 937–942.
[39] H.T. Xu, N.W. Zheng, H.H. Xu, Y.G. Wu, R.Y. Yang, E.Y. Ye, X.L. Jin, J. Mol. Struct. 597 (2001) 1–5.
[40] L.L. Wen, Z.D. Lu, J.G. Lin, Z.F. Tian, H.Z. Zhu, Q.J. Meng, Cryst. Growth Des. 7 (2007) 93–99.
[41] Y.L. Wei, H.W. Hou, L.K. Li, Y.T. Fan, Y. Zhu, Cryst. Growth Des. 5 (2005) 1405–1413.
[42] Y.S. Song, B. Yan, L.H. Weng, Inorg. Chem. Commun. 9 (2006) 567–570.
[43] Y.C. Liang, M.C. Hong, W.P. Su, R. Cao, W.J. Zhang, Inorg. Chem. 40 (2001) 4574–4582.
[44] Y.C. Liang, R. Cao, W.P. Su, M.C. Hong, W.J. Zhang, Angew. Chem. Int. Ed. 39 (2000) 3304–3307.
[45] W. Lin, O.R. Evans, R.G. Xiong, Z. Wang, J. Am. Chem. Soc. 120 (1998) 13272–13273.
[46] G.B. Garder, D. Venkataraman, J.S. Moore, Nature 374 (1995) 792–795.
[47] O.R. Evans, R.G. Xiong, Z.Y. Wang, K.W. George, W.B. Lin, Angew. Chem. Int. Ed. 38 (1999) 536–538.
[48] M.L. Tong, L.J. Li, K. Mochizuki, H.C. Chang, X.M. Chen, Y. Li, S. Kitagawa, Chem. Commun. (2003) 428–429.
[49] R.G. Xiong, J. Zhang, Z.F. Chen, X.Z. You, C.M. Che, H.K. Fun, J. Chem. Soc. Dalton Trans. (2001) 780–782.
[50] C.M. Liu, S. Gao, H.Z. Kou, Chem. Commun. (2001) 1670–1671.
[51] G.M. Sheldrick, SHELXTL, Crystallographic Software Package, Version 5.1, Bruker-AXS, Madison, WI, 1998.
[52] L.J. Bellamy, The Infrared Spectra of Complex Molecules, Wiley, New York, 1958.
[53] G.Q. Zhang, G.Q. Yang, J.S. Ma, Cryst. Growth Des. 6 (2006) 933–939.
[54] O.L. Malta, M.A. Couto dos Santos, L.C. Thompson, N.K. Ito, J. Lumin. 69 (1996) 77–84.
[55] O.L. Malta, H.F. Brito, J.F.S. Menezes, F.R. Gonçalves e Silva, S. Alves Jr., F.S. Farias Jr., A.V.M. Andrade, J. Lumin. 75 (1997) 255–268.
[56] M.H.V. Werts, R.T.F. Jukes, J.W. Verhoeven, Phys. Chem. Chem. Phys. 4 (2002) 1542–1548.